Applied Surface Science 255 (2009) 6195–6200

Contents lists available at ScienceDirect

Applied Surface Science

journal homepage: www.elsevier.com/locate/apsusc

Dependence of film thickness on the structural and optical properties of ZnO thin films

Ebru Şenadım Tüzemen [a,*], Sıtkı Eker [b], Hamide Kavak [c], Ramazan Esen [c]

[a] Department of Physics, Cumhuriyet University, 58140 Sivas, Turkey
[b] Department of Physics, University of Ahi Evran, 40100 Kırşehir, Turkey
[c] Department of Physics, Çukurova University, 01330 Adana, Turkey

ARTICLE INFO

Article history:
Received 19 November 2008
Received in revised form 21 January 2009
Accepted 23 January 2009
Available online 3 February 2009

PACS:
78.20−e
78.20.Ci
81.05.Dz
81.15.Ef

Keywords:
X-ray diffraction
Optical microscopy
Semiconducting II–VI materials
Kramers–Kronig and dispersion relations

ABSTRACT

ZnO thin films are prepared on glass substrates by pulsed filtered cathodic vacuum arc deposition (PFCVAD) at room temperature. Optical parameters such as optical transmittance, reflectance, band tail, dielectric coefficient, refractive index, energy band gap have been studied, discussed and correlated to the changes with film thickness. Kramers–Kronig and dispersion relations were employed to determine the complex refractive index and dielectric constants using reflection data in the ultraviolet–visible–near infrared regions. Films with optical transmittance above 90% in the visible range were prepared at pressure of 6.5×10^{-4} Torr. XRD analysis revealed that all films had a strong ZnO (0 0 2) peak, indicating *c*-axis orientation. The crystal grain size increased from 14.97 nm to 22.53 nm as the film thickness increased from 139 nm to 427 nm, however no significant change was observed in interplanar distance and crystal lattice constant. Optical energy gap decreased from 3.21 eV to 3.19 eV with increasing the thickness. The transmission in UV region decreased with the increase of film thickness. The refractive index, Urbach tail and real part of complex dielectric constant decreased as the film thickness increased. Oscillator energy of as-deposited films increased from 3.49 eV to 4.78 eV as the thickness increased.
© 2009 Elsevier B.V. All rights reserved.

1. Introduction

Zinc oxide (ZnO) films with a hexagonal wurtzite structure have a wide direct band gap of 3.3 eV at room temperature and high transmittance for visible light. Because of this feature zinc oxide is a very interesting material for many different applications. The optical properties of ZnO have received increasing attention recently due to the promising applications of this material in short wavelength optoelectronic devices as well as low voltage phosphors in flat panel display [1,2].

Several techniques have been used to fabricate ZnO films, including electrochemical deposition (ECD) technique [3], thermal oxidation [4], MOCVD [5], r.f. magnetron sputtering [6], pulsed laser deposition [7] and MBE [8].

Pulsed filtered cathodic vacuum arc deposition (PFCVAD) is a common method to prepare oxide. This arc source provides particles of high ionization rate and high ion energy (50–150 eV) for condensation on substrate. The films usually adhere well due to the induced ion mixing by the bombardment of energetic particles. Recently, polycrystalline ZnO semiconductor thin films produced by FCVAD have been reported [9,10].

The characteristics of ZnO films are affected by the preparation conditions such as deposition pressure, substrate temperature, types of substrates, thickness of the films, and annealing temperature. Among these factors, the influence of thickness on the characteristics of ZnO thin films is less reported.

In this study, ZnO thin films were deposited by PFCVAD on glass substrates. The direct influence of film thickness on the structural and optical properties of ZnO thin films is investigated.

2. Experimental details

2.1. Sample preparation and characterization

The details of the PFCVAD system have been described elsewhere [10]. The cylindrical vacuum chamber was made of stainless steel (486 mm diameter and 385 mm in length) and evacuated using a primary and a turbomolecular pump (500 lt/s) to a base pressure below 1.3×10^{-8} Torr.

In these study deposition parameters for ZnO thin film as follows: oxygen gas flow rate 135 sccm, oxygen pressure during

* Corresponding author. Tel.: +90 346 219 1010x1397.
E-mail addresses: esenadim@cumhuriyet.edu.tr, Ebru_Senadim@hotmail.com (E.zemen).

0169-4332/$ – see front matter © 2009 Elsevier B.V. All rights reserved.
doi:10.1016/j.apsusc.2009.01.078

the deposition 6.5×10^{-4} Torr, in fixed arc current of 650 A, substrate temperature room temperature. The distance from the target to the substrate was maintained to be 14 mm. The PFCVAD ZnO thin films were deposited on glass substrates at the same condition but different thicknesses and were labeled as ZnO1 (139 nm), ZnO2 (227 nm), ZnO3 (427 nm).

X-ray diffraction technique was used to specify the structural parameters, the existent phases and the orientation of ZnO thin films. The X-ray diffraction measurements were performed by using a Rigaku Miniflex X-ray diffraction system equipped with Cu Kα radiation of average wavelength 1.54059 Å. X-ray diffractograms was taken 2θ is in between 20° and 70° and scan speed of 2°/min.

The optical properties of ZnO thin films deposited by PFCVAD were carried out with a double beam computer controlled spectrophotometer (PerkinElmer Lambda 2S) in the UV/VIS/NIR regions. The optical transmittance and absorbance at normal incidence were recorded in the wavelength range of 190–1100 nm. The absorption coefficient α was determined from absorption spectra.

Kramers–Kronig relation was employed to evaluate the refractive index n as a function of wavelength. The thickness of ZnO films were optically measured by Filmetrics F30. And also the thickness was determined from interference fringes of transmission data measured over the visible range.

2.2. Kramers–Kronig and dispersion analysis

The Kramers–Kronig relations are based upon the fundamental notions of linearity and causality [11]. The relations can be used to connect the attenuation coefficient and phase velocity of a material and also provide a criterion for the causal consistency of a measurement or model of the propagation mechanisms. K–K transformation are commonly used to determine index of refraction n and extinction coefficient versus wavelength from the reflectance spectra [12–14]. For solid materials, if $R(\lambda)$ and $\theta(\lambda)$ are known, the refractive index $n(\lambda)$ and extinction coefficient $k(\lambda)$ of that material are given by

$$n(\lambda) = \frac{1 - R(\lambda)}{1 + R(\lambda) - 2\sqrt{R(\lambda)}\cos(\theta(\lambda))}, \tag{1}$$

$$k(\lambda) = -\frac{2\sqrt{R(\lambda)}\sin(\theta(\lambda))}{1 + R(\lambda) - 2\sqrt{R(\lambda)}\cos(\theta(\lambda))}, \tag{2}$$

where $R(\lambda)$ is the measured reflectance spectrum, λ is the wavelength and $\theta(\lambda)$ is the phase shift arising from the reflection. By taking logarithm of $\hat{r}(\lambda) = \sqrt{R(\lambda)}e^{i\theta(\lambda)}$, one obtains

$$\ln(\hat{r}(\lambda)) = \ln[\sqrt{R(\lambda)}] + i\theta(\lambda) \tag{3}$$

If Hilbert transformation is applied to this expression, the real and imaginary parts of it can be related to each other as

$$\theta(\lambda_m) = \frac{2\lambda_m}{\pi} \times \left[\int_0^a \frac{\ln\sqrt{R(\lambda)}d\lambda}{\lambda^2 - \lambda_m^2} + \int_a^b \frac{\ln\sqrt{R(\lambda)}d\lambda}{\lambda^2 - \lambda_m^2} + \int_b^\infty \frac{\ln\sqrt{R(\lambda)}d\lambda}{\lambda_m^2}\right] \tag{4}$$

Moreover, the complex dielectric constant of a solid is given as

$$\hat{\varepsilon}(\lambda) = \varepsilon_1(\lambda) + i\varepsilon_2(\lambda) \tag{5}$$

Here, real and imaginary parts are related to $n(\lambda)$ and $k(\lambda)$ as

$$\varepsilon_1(\lambda) = n^2(\lambda) - k^2(\lambda) \tag{6}$$

$$\varepsilon_2(\lambda) = 2n(\lambda)k(\lambda) \tag{7}$$

In the normal dispersion region (the transparent region), the refractive index dispersion has been analyzed using the single-oscillator model developed by Wemple and DiDomenico [15,16]. According to this model, the relation between the refractive index n and photon energy E can be written as follows:

$$n = \left[1 + \frac{E_{osc}E_d}{E_{osc}^2 - (E)^2}\right]^{1/2} \tag{8}$$

where E_{osc} is the single-oscillator energy and E_d is the dispersion energy.

Dispersion energy E_d obeys a simple empirical relationship as $E_d = \beta N_c Z_a N_e$ eV. In this equation, N_c is the coordination number of the nearest-neighbor cation, Z_a is the formal anion valence, and N_e is the effective number of valence electron per anion. β is the constant and can find using the published data for N_c, Z_a and N_e [15].

3. Results and discussion

3.1. X-ray diffraction results

Fig. 1 shows the X-ray diffraction pattern for ZnO thin films with different film thickness. Different thickness of ZnO1 (139 nm), ZnO2 (227 nm), and ZnO3 (427 nm) thin films were deposited on glass substrate at 6.5×10^{-4} Torr oxygen pressure. An XRD spectrum as shown in Fig. 1 reveals the influence of thickness on the structure of the ZnO thin film. For all the films only the ZnO (0 0 2) peak is observed, indicating that the films are polycrystalline with a hexagonal structure and a preferred orientation with the c-axis perpendicular to the substrate. From the peak position of the (0 0 2) peak, the grain size, the full width at half maximum (FWHM), interplanar distance d, stress σ, strain ε_z and crystal lattice constant c are calculated.

According to Fig. 1, diffraction peaks (2θ) and FWHM for ZnO1, ZnO2, ZnO3 thin films have the values of 34.28°, 34.38°, 34.42° and 0.555°, 0.369°, 0.369°, respectively. This means that the quality of films was determined by the ZnO thin films thickness. Fig. 1 also shows that as the film thickness increases the diffraction peaks become sharper, their intensity is enhanced and its location changes. This behavior means that residual stresses are generated during the deposition process.

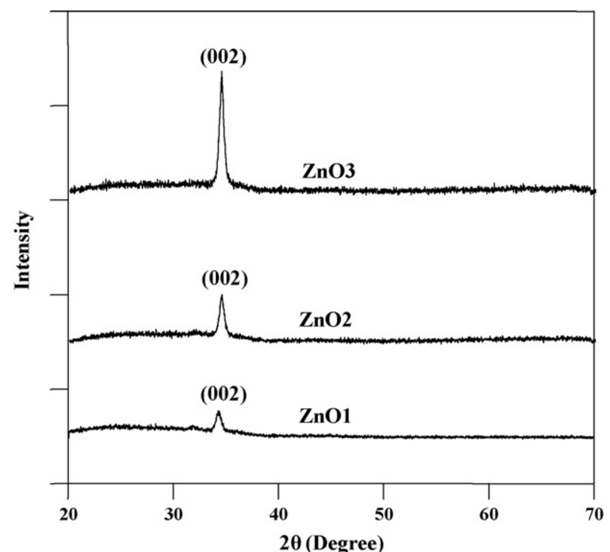

Fig. 1. The X-ray diffraction spectra of as-deposited ZnO thin films with different thickness.

Table 1
X-ray diffraction data summary of ZnO thin films with different film thickness grown by pulsed filtered cathodic vacuum arc deposition.

	ZnO1	ZnO2	ZnO3
Thickness (nm)	139	227	427
2θ (°)	34.28	34.38	34.42
Relative peak intensity	681	1248.33	2863.33
FWHM (°)	0.555	0.369	0.369
Grain size (nm)	14.97	22.52	22.53
c (nm)	0.522	0.521	0.520
d (nm)	0.2612	0.2605	0.2602
ε_z (%)	0.257	0.0653	−0.126
Stress, σ ($\times 10^9$ Pa)	−0.599	−0.152	0.295

The strain in the ZnO films along c-axis perpendicular to substrate are given by the following equation [17]

$$\varepsilon_z\,(\%) = \frac{c - c_0}{c_0} \times 100$$

where c is the lattice parameter of the ZnO film, c_0 (5.2066 Å) is the unstrained lattice parameter of ZnO [17]. The values of the strain for ZnO1, ZnO2 and ZnO3 thin films are given in Table 1. The strain can be positive (tensile) or negative (compressive).

The residual stress (σ) in ZnO films can be expressed as [18]

$$\sigma = \frac{2c_{13}^2 - c_{33}(c_{11} + c_{12})}{2c_{13}} \times \frac{c - c_0}{c_0}.$$

Here c_{ij} are the elastic stiffness constants for single crystal ZnO (c_{11} = 208.8 GPa, c_{33} = 213.8 GPa, c_{12} = 119.7 GPa and c_{13} = 104.2 GPa [19]). The residual stress with increasing the thickness increases. The values of the residual stress for ZnO1, ZnO2 and ZnO3 thin films are given in Table 1. If the stress is positive, the biaxial stress is tensile; if the stress is negative, the biaxial stress is compressive [20]. The residual stresses of ZnO1 and ZnO2 thin films are compressive. The residual stress of the ZnO3 thin film is tensile.

The crystal sizes of ZnO thin films with different thicknesses were calculated using Scherrer's formula [21,22]:

$$D = \frac{0.9\lambda}{\beta \cos\theta},$$

where λ = 1.54 Å and β FWHM were determined from the broadening of the ZnO diffraction line.

The crystal lattice constant c and the interplanar distance of the diffracting planes d were identified using Bragg's equation $n\lambda = 2d \sin\theta$, where n is the order of the diffracted beam, λ is the wavelength of the X-ray and θ is the angle between the incoming X-ray and the normal of the diffracting plane. The values of peak position, peak intensity, FWHM, grain size, lattice constant c and interplaner distance d for different thickness of ZnO1, ZnO2, and ZnO3 films were reported in Table 1. The grain size and the crystalline quality increased with the increase of film thickness. No significant changes in the values of c and d were observed with the change of the film thickness.

3.2. The thickness dependence of optical properties

The absorption coefficient α was calculated by

$$T = (1 - R)^2 \exp(-\alpha t)$$

where T is the transmittance of the thin film, R is the reflectance and t is the thickness of the film. Since the reflectivity is negligible and insignificant near the absorption edge this relation simply to the following relation:

$$\alpha = \frac{1}{t}(2.3 * A) \tag{9}$$

where A is the absorbance and t is the thickness of the film. The thickness of the zinc oxide thin film was evaluated from the interference fringes and this value is verified with a Filmetrics instrument. From the interference fringes, the thickness t of the film was calculated using the following relation:

$$t = \frac{\lambda_1 \lambda_2}{2[n(\lambda_1)\lambda_2 - n(\lambda_2)\lambda_1]} \tag{10}$$

where $n(\lambda_1)$ and $n(\lambda_2)$ are the refractive indices at the two adjacent maxima (or minima) at λ_1 and λ_2.

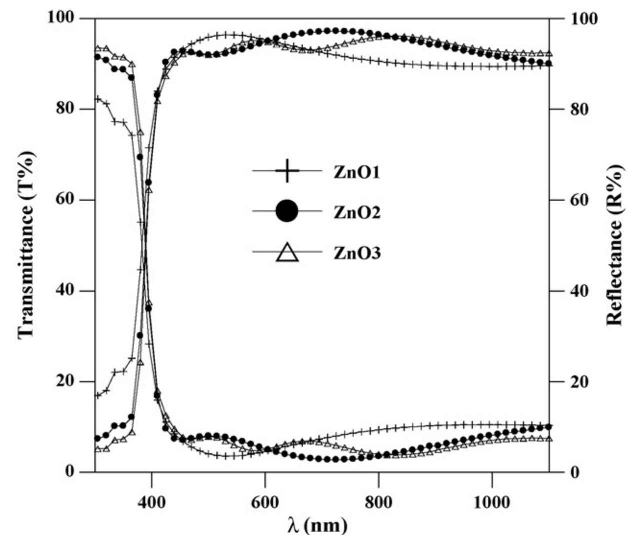

Fig. 2. The transmittance and reflection spectra of ZnO thin films for different thickness.

Fig. 2 presents the optical transmittance and reflectance in the wavelength range of 300–1100 nm for the ZnO1, ZnO2, and ZnO3 thin films. The average transmittance in the visible part of the spectra (400–700 nm) was over 90%, for all the samples analyzed. With increasing film thickness, the transmittance of the films is decreased due to the thickness effect. These changes of the transmittances are associated to the increase of the carrier concentration [23]. By comparison, the absorption edge was observed at a slightly lower wavelength range for ZnO1 film. The shift of absorption edge may be attributed to the difference in grain size [24] and/or carrier concentration [25,26]. From the results of XRD (Fig. 1), ZnO1 thin film with 139 nm thickness contained relatively small grain size; this was probably why the blue shift occurred. It suggested that the grain size indeed affects the optical properties significantly. A comparison of ZnO1 sample with ZnO3, ZnO3 shows that thinner film has higher optical energy gap, smaller grain size, and shows the blue shift. The corresponding values of absorption edge have been given in Table 2.

To determine the optical band gap E_g, we have used Tauc et al.'s plot [27] where the absorption coefficient α is a parabolic function of the incident photon energy ($h\nu$) and optical band gap E_g. This relation is given by

$$\alpha = \frac{A(h\nu - E_g)^{1/2}}{h\nu} \tag{11}$$

where A is function of refractive index of the material, reduced mass and speed of light.

Table 2
Thickness dependent optical properties of ZnO thin films.

Sample	Thickness (nm)	Absorption edge (nm)	Energy gap (eV)	Urbach tail E_0 parameter (eV)
ZnO1	139	397	3.21	0.153
ZnO2	227	400	3.20	0.122
ZnO3	427	403	3.19	0.114

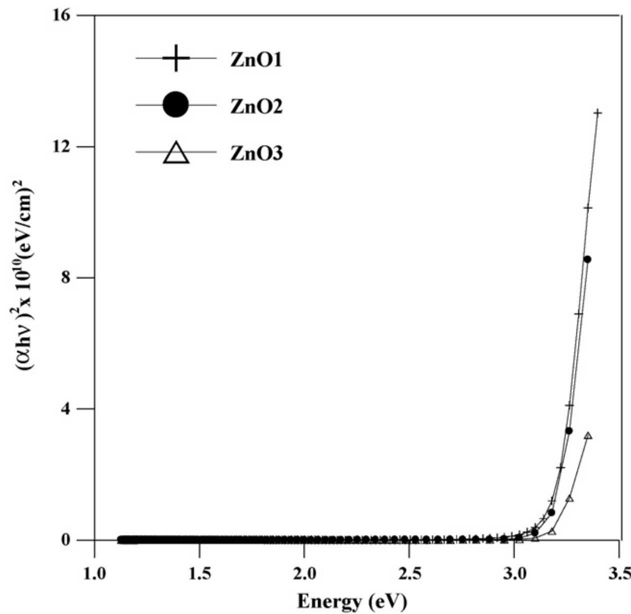

Fig. 3. Variation of $(\alpha h\nu)^2$ with photon energy $(h\nu)$ of ZnO thin films as a function of film thickness.

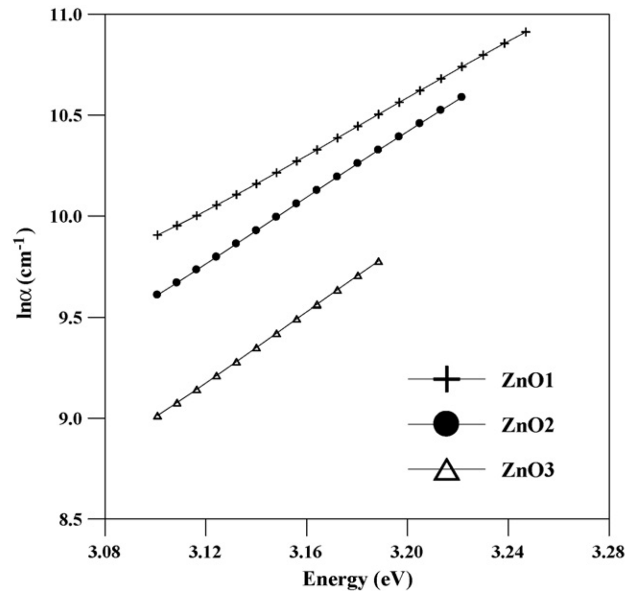

Fig. 4. Semi-logarithmic plots of absorption coefficient as a function of energy for the ZnO thin film of different thickness.

The plot of $(\alpha h\nu)^2$ as a function of the energy of incident radiation has been shown in Fig. 3. The energy band gap is obtained from intercept of the extrapolated linear part of the curve with the energy axis. The optical energy band gap of the films decreased from 3.21 eV to 3.19 eV as the thickness increased from 139 nm to 427 nm. The corresponding values of E_g have been given in Table 2.

According to Tauc et al. [27] it is possible to separate three distinct regions in the absorption edge spectrum. The first is the weak absorption tail region, the second is the exponential edge region and the third is the high absorption region. In the exponent edge where the absorption coefficient α lies in the absorption region of $1 < \alpha < 10^4$ cm^{-1}, the absorption coefficient is governed by the relation [28],

$$\alpha = AE_0^{3/2} \exp\left(\frac{h\nu}{E_0}\right) \quad \text{for } h\nu < E_g \tag{12}$$

where E_0 is an empirical parameter describing the width of the localized states in the band gap due to above mention effects.

Fig. 4 illustrates the semi-logarithmic plot of absorption coefficient α as function of E in the photon energy region where $\alpha < 10^4$ cm^{-1}. The value of Urbach tail energy E_0 is calculated from the slope of this the linear plot. From this figure it is clear that defects decrease sharply with increasing the thickness and the value of E_0 has been also listed in Table 2.

Kramers–Kronig analysis has been applied for ZnO thin films with different thickness by using the reflectance data as plotted in Fig. 2. By substituting these phase values and experimental reflectance data in Eqs. (1)–(4), $n(\lambda)$ is calculated. Fig. 5 shows the changes of refractive index of the ZnO thin films in the wavelength range of 300–1100 nm under various thicknesses. For the all samples, the refractive index decreases with the increasing of wavelength in the visible region. The refractive index increases in the wavelength range from 300 nm, 300 nm, and 300 nm to 368 nm, 366 nm and, 364 nm for ZnO1, ZnO2 and ZnO3 thin films, respectively. But the refractive index decreases when increasing film thickness in the wavelength range from 368 nm, 366 nm, and 364 nm to 1100 nm.

Real part of dielectric function $\varepsilon_1(\lambda)$ was determined employing Eq. (6) and a plot of $\varepsilon_1(\lambda)$ as a function of wavelength was shown in Fig. 6. It can be seen that the real part of the dielectric constant decreases with increasing wavelength in the visible region while increases in the ultraviolet region. The real part of the dielectric constant decreases with increasing film thickness in the visible region.

Using single-oscillator model refractive index energy relation (Eq. (8)), the single-oscillator energy E_{osc} and the dispersion energy E_d can be determined by plotting $(n^2 - 1)^{-1}$ against E^2. From Fig. 7, the equations for the best fitting straight line are given as

$$\frac{1}{n(E)^2 - 1} = -378 \times 10^{-4}E^2 + 0.46 \,(\text{for ZnO1}),$$

$$\frac{1}{n(E)^2 - 1} = -317 \times 10^{-4}E^2 + 0.69 \,(\text{for ZnO2}),$$

$$\frac{1}{n(E)^2 - 1} = -367 \times 10^{-4}E^2 + 0.84 \,(\text{for ZnO3}).$$

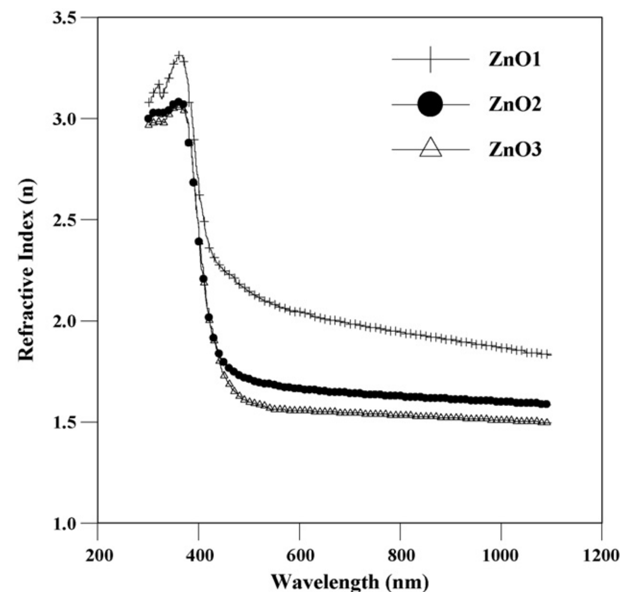

Fig. 5. Dependence of the refractive index (n) with wavelength for different thicknesses of ZnO thin films.

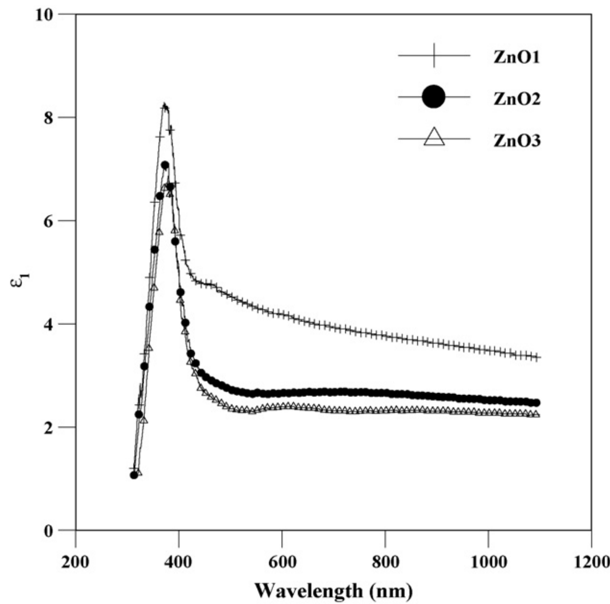

Fig. 6. Real (ε_1) parts of the dielectric function as function of thewavelength for different thicknesses of ZnO thin films.

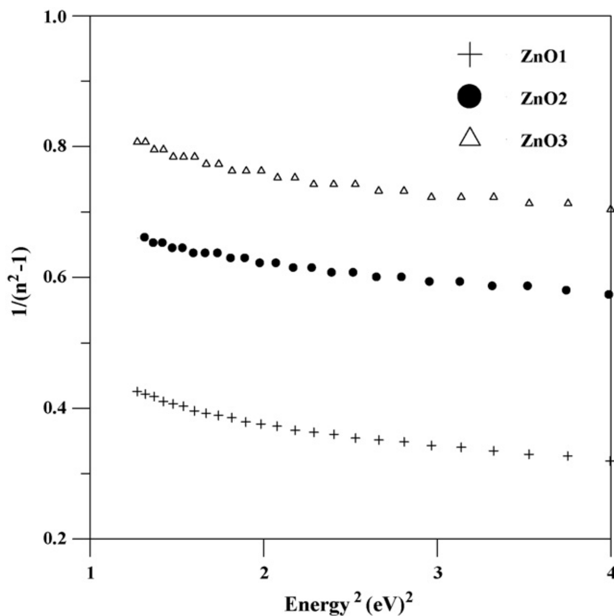

Fig. 7. Plot of $1/(n^2-1)$ versus photon energy squared for different thicknesses of ZnO thin films.

Oscillator parameters E_d and E_{osc} are obtained from the intercepts and the slopes of the lines in the plot. These values have been listed in Table 3. As seen in this table oscillator energy E_{osc} increased as the film thickness increased and approached to value of $E_{osc} = 2E_g$, while dispersion energy E_d and β decreased.

Table 3
Oscillator parameters of ZnO thin films with different film thickness.

Sample	Thickness (nm)	E_d (eV)	E_{osc} (eV)	β (eV)	λ_0 (nm)	n_∞	ε_∞
ZnO1	139	7.58	3.49	0.118	356	1.78	3.18
ZnO2	227	6.76	4.67	0.106	265.5	1.56	2.45
ZnO3	427	5.70	4.78	0.089	259.1	1.48	2.19

Table 4
The comparison results of this study with the published data.

References	Grain size (nm)	Energy gap (eV)
In this study	14.97–22.53	3.19–3.21
[30]	23–38	3.19–3.24
[31]	25–75	–
[32]	15–25	–
[3]	23.5–31	–
[33]	18–48	–
[34]	–	3.25–3.33
[35]	–	3.28–3.29

The obtained data of refractive index (n) can be analyzed to yield the long wavelength refractive index (n_∞) together with the average oscillator wavelength (λ_0) for ZnO thin film using the following relation [29]:

$$\frac{n_\infty^2 - 1}{n^2 - 1} = 1 - \left(\frac{\lambda_0}{\lambda}\right)^2 \tag{13}$$

where λ_0 and n_∞ can be evaluated from plots of $(n^2 - 1)^{-1}$ against λ^{-2}. The value of $n_\infty^2 = \varepsilon_\infty$ was given in Table 3.

Table 4 shows some results of ZnO thin films by comparing with the published data; we conclude that pulsed filtered cathodic vacuum arc deposition is a suitable film deposition technique to obtain very similar properties.

4. Conclusions

ZnO films were deposited on glass substrate by pulsed filtered cathodic vacuum arc (PFCVAD) at room temperature. The structural and optical properties of the ZnO films are found to be dependent on the film thickness. The crystal structure of the ZnO films is hexagonal wurtzite and the films are highly oriented along the c-axis perpendicular to the substrates. As film thickness increases, the crystallinity is improved and the crystallite sizes become larger.

The average transmittance for all prepared samples is over 90% in the wavelength range of the visible spectrum and the transmission in UV region decreased with the increase of film thickness. Such behavior was due to the films with different thickness showing different structural properties. The optical energy band gap E_g is dependent on the film thickness. For the thinner samples the optical energy band gap is higher. This may be due to different effects, but the most relevant are grain size, lattice strain or defect states. The refractive index n, Urbach tail parameters and real part of the complex dielectric constant ε_1 decreased as the film thickness increased.

The dispersion of the refractive index in the transparent region is interpreted successfully using a single-oscillator model; oscillator energy and dispersion energy were obtained for different thickness of ZnO thin films. Oscillator energy increases as the film thickness increases. These results demonstrate that good quality ZnO thin films can be deposited by using the pulsed filtered cathodic vacuum arc technique.

Acknowledgments

This work was supported by the Scientific and Technological Research Council of Turkey under Grant No 106T613. The author would like to thank H. Karaağaç for the XRD analysis.

References

[1] C.G. Van de Walle, Physica B 308–310 (2001) 899.
[2] D.C. Look, Mater. Sci. Eng. B 80 (2000) 383.

[3] E. Gür, H. Asıl, C. Coşkun, S. Tüzemen, K. Meral, Y. Onganer, K. Şerifoğlu, Nucl. Instrum. Methods Phys. Res. B 266 (2008) 2021.
[4] X.T. Zhang, Y.C. Liu, Z.Z. Zhi, J.Y. Zhang, Y.M. Lu, D.Z. Shen, X.W. Fan, X.G. Kong, J. Lumin. 99 (2002) 149.
[5] A. Dadgar, et al. J. Crystal Growth 267 (2004) 140.
[6] Q.P. Wang, X.J. Zhang, G.Q. Wang, S.H. Chen, X.H. Wu, H.L. Ma, Appl. Surf. Sci. 254 (2008) 5100.
[7] X.Q. Wei, Z.G. Zhang, M. Liu, C.S. Chen, G. Sun, C.S. Xue, H.Z. Zhuang, B.Y. Man, Mater. Chem. Phys. 101 (2007) 285.
[8] X. Wang, H. Iwaki, M. Murakami, X. Du, Y. Ishitani, A. Yoshikawa, Jpn. J. Appl. Phys. 42 (2003) L99.
[9] Y.G. Wang, S.P. Lau, H.W. Lee, S.F. Yu, B.K. Tay, X.H. Zhang, K.Y. Tse, H.H. Hng, J. Appl. Phys. 94 (3) (2003) 1597.
[10] E. Şenadım, H. Kavak, R. Esen, J. Phys.: Condens. Matter 18 (2006) 6391.
[11] K.R. Waters, M.S. Hughes, J. Mobley, G.H. Brandenburger, J.G. Miller, J. Acoust. Soc. Am. 108 (2000) 556.
[12] M.G. Sceats, G.C. Morris, Phys. Status Solidi A 14 (1972) 643.
[13] F.W. King, J. Chem. Phys. 71 (11) (1979) 4726.
[14] B. Harbecke, Appl. Phys. A 40 (1986) 151.
[15] S.H. Wemple, M. DiDomenico, Phys. Rev. B 3 (1971) 1338.
[16] S.H. Wemple, M. DiDomenico, Phys. Rev. Lett. 23 (1969) 1156.
[17] H.C. Ong, A.X.E. Zhu, G.T. Du, Appl. Phys. Lett. 80 (2002) 941.
[18] C. Wang, P. Zhang, J. Yue, Y. Zhang, L. Zheng, Physica B 403 (2008) 2235.
[19] B.D. Cullity, Elements of X-ray Diffractions, Addison-Wesley, Reading, MA, 1978.
[20] C. Li, X.C. Li, P.X. Yan, E.M. Chong, Y. Liu, G.H. Yue, X.Y. Fan, Appl. Surf. Sci. 253 (2007) 4000.
[21] L. Sagalowicz, G.R. Fox, J. Mater. Res. 14 (5) (1999) 1876.
[22] G. Sanon, R. Rup, A. Mansingh, Thin Solid Films 190 (1990) 287.
[23] T.J. Coutts, D.L. Young, X. Li, MRS Bull. 25 (2000) 58.
[24] J. Yu, X. Zhao, Q. Zhao, Thin Solid Films 379 (2000) 7.
[25] W. Tang, D.C. Cameron, Thin Solid Films 238 (1994) 83.
[26] B.E. Sernelius, K.F. Berggren, Z.C. Jin, I. Hamberg, C.G. Granqvist, Phys. Rev. B 37 (1998) 10244.
[27] J. Tauc, R. Grigorvici, Y. Yanca, Phys. Status Solidi 15 (1966) 627.
[28] J.I. Pankove, Phys. Rev. 140 (1965) A2059.
[29] T.S. Moss, Optical Properties of Semiconductors, Butterworth, London, 1959.
[30] T. Prasada Rao, M.C. Santhoshkumar, Appl. Surf. Sci. 255 (2009) 4579.
[31] V. Khranovskyy, A. Ulyashin, G. Lashkarev, B.G. Svensson, R. Yakimova, Thin Solid Films 516 (2008) 1396.
[32] X. Teng, H. Fan, S. Pan, C. Ye, G. Li, Mater. Lett. 61 (2007) 201.
[33] Y. Zhang, G. Du, D. Liu, X. Wang, Y. Ma, J. Wang, J. Yin, X. Yang, X. Hou, S. Yang, J. Crystal Growth 243 (2002) 439.
[34] L.W. Lai, C.T. Lee, Mater. Chem. Phys. 110 (2008) 393.
[35] U. Choppali, B.P. Gorman, J. Lumin. 128 (2008) 1641.